NANO LETTERS

2008
Vol. 8, No. 6
1649-1653

Solution-Processed Ultraviolet Photodetectors Based on Colloidal ZnO Nanoparticles

Yizheng Jin,[†,‡] Jianpu Wang,[†] Baoquan Sun,[†] James C. Blakesley,[†] and Neil C. Greenham*[,†]

Cavendish Laboratory, JJ Thomson Avenue, Cambridge, CB3 0HE, United Kingdom, and State Key Laboratory of Silicon Materials, Zhejiang University, Hangzhou, 310027, China

Received February 6, 2008; Revised Manuscript Received April 11, 2008

ABSTRACT

A "visible-blind" solution-processed UV photodetector is realized on the basis of colloidal ZnO nanoparticles. The devices exhibit low dark currents with a resistance >1 TΩ and high UV photocurrent efficiencies with a responsivity of 61 A/W at an average intensity of 1.06 mW/cm^2 illumination at 370 nm. The characteristic times for the rise and fall of the photocurrent are <0.1 s and about 1 s, respectively. The photocurrent of the device is associated with a light-induced desorption of oxygen from the nanoparticle surfaces, thus removing electron traps and increasing the free carrier density which in turn reduces the Schottky barrier between contacts and ZnO nanoparticles for electron injection. The devices are promising for use in large-area UV photodetector applications.

Ultraviolet (UV) photodetectors have a wide range of applications both in civilian and military areas, including flame sensing, environmental and biological research, astronomical studies, optical communication, missile launch detection, and so forth.[1] "UV-enhanced" silicon photodiodes, the most common devices for UV photodetection, exhibit some inherent limitations: the requirement for filters to block out visible and infrared photons, and degradation of devices on exposure to UV light with energies much higher than the semiconductor bandgap. For high-sensitivity applications, silicon photodiodes need to be cooled to reduce the dark current.

Advances in wide-bandgap semiconductors, such as GaN, SiC, and so forth, show the possibility of developing photodetectors with intrinsic "visible-blindness" and enable room-temperature operation.[1–5] Among them, ZnO, an environmentally friendly semiconductor with a room-temperature band gap of 3.35 eV, is of great interest for UV detection because of its various synthetic methods, diverse processing technologies, and the capability of operating at high temperatures and in harsh environments. Liu et al. fabricated Schottky UV photodetectors which exhibit fast response speed (microsecond scale) by growing high quality ZnO epitaxial films on sapphire substrates.[6] Nevertheless, achieving high crystal quality of ZnO thin films with suitable metal contacts is still challenging because of the lack of high-quality and low-cost substrates for lattice-matched growth. Most ZnO thin films deposited by metal−organic chemical vapor deposition, pulsed laser deposition, or radio frequency sputtering have a large density of dislocations and grain boundaries. Transport and UV photoconduction in these polycrystalline ZnO films depends sensitively on stoichiometry, trap densities, and most importantly, gas adsorption and desorption on the crystal surfaces. A slow response time of UV photodetectors based on polycrystalline ZnO thin films, ranging from a few minutes to several hours, is commonly observed.[7–13] Recently, ZnO nanowires produced by chemical vapor deposition technology have been investigated by several groups for UV photodetector applications.[14–19] Their results show that, for a range of different synthesis conditions and device processing, the conductivities of ZnO nanowires are sensitive to UV light exposure. However, ZnO nanowire devices are created using time-consuming nanowire manipulation methods and one-by-one fabrication techniques, making them unattractive for large-scale production.

Solution-processed electronic and optoelectronic devices have some advantages over conventional crystalline semiconductor devices in terms of ease of fabrication, large device area, physical flexibility, and most importantly, low cost.[20–23] The development of synthesis strategies for colloidal ZnO nanocrystals paves the way toward solution-processed ZnO nanocrystalline devices.[24,25] ZnO nanoparticle/conjugated polymer blends have been employed as light-sensitive layers

* Corresponding author. E-mail: ncg11@cam.ac.uk.
† Cavendish Laboratory.
‡ Zhejiang University.

10.1021/nl0803702 CCC: $40.75
Published on Web 05/07/2008

in photovoltaic cells, and power conversion efficiencies of 1.2% were achieved.[25,26] High-performance n-type field effect transistors have been fabricated from self-assembly of colloidal ZnO nanorods and field effect mobilities up to 1.2−1.4 $cm^2\ V^{-1}\ s^{-1}$ were demonstrated.[27,28]

Here, we report the fabrication of "metal−semiconductor−metal" UV photodetectors by spin-coating colloidal ZnO nanoparticles on glass substrates, followed by annealing in air and evaporation of gold contacts through a shadow mask. (Experimental details are presented as Supporting Information.) The device structure is depicted in Figure 1a. Figure 1b shows UV−vis spectra of both an as-prepared ZnO nanoparticle solution and a spin coated ZnO nanoparticle film after annealing. Because of the quantum confinement effect, the as-prepared ZnO nanoparticles have a blue-shifted absorbance peak at approximately 340 nm compared with that of bulk ZnO, which has an absorbance peak at 370 nm corresponding to a 3.35 eV bandgap at room temperature. After annealing, the ZnO film exhibits an absorbance onset at approximately 355 nm, suggesting a certain degree of particle sintering or necking between abutting nanoparticles in the annealing process. Figure 1c shows the photocurrent spectral response at 50 V of a ZnO nanoparticle film device. The photocurrent shows a sharp onset from 400 nm, and little photoresponse is found in the range from 400 to 700 nm. The high spectral selectivity suggests that the ZnO nanoparticle film device is intrinsically "visible-blind".

Figure 2a shows typical $I-V$ characteristics of a ZnO nanoparticle film device both in the dark and upon 0.83 mW/cm^2 UV light illumination ($\lambda = 370$ nm). The initial annealed ZnO nanoparticle film is very resistive in the dark. Up to $V_{bias} = 120$ V, a small current (<120 pA) flows in the device, which corresponds to a resistance $R > 1$ TΩ at room temperature. It is noteworthy that the dark current of a ZnO nanoparticle film depends strongly on the stoichiometry of the ZnO nanoparticles which is determined by the molar ratio between KOH and zinc acetate in the synthesis, as pointed out by Sun et al.[27] The current increases by nearly 6 orders of magnitude upon 1.06 mW/cm^2 UV illumination (average power density), indicating a highly UV-sensitive photoconduction. The $I-V$ curve under illumination is linear when $V_{bias} < 40$ V and then follows an exponential rise at higher biases. The intensity dependence of the photocurrent in a ZnO nanoparticle film device is shown in Figure 2b. The photocurrent of the device increases by nearly 4 orders of magnitude from 34 nA to 3.1 × 10^5 nA as the average light intensity is increased from 10.3 μW/cm^2 to 1.06 mW/cm^2. The photocurrent, I_{pc}, follows a power-law relationship with intensity, P: $I_{pc} \propto P^{1.9}$. The responsivity of the device, defined as photocurrent per unit of incident optical power, has been determined to be approximately 61 A/W at intensities of 1.06 mW/cm^2 (370 nm). For comparison, the responsivity of most commercial UV photodetectors is in the range of 0.1 to 0.2 A/W.[1] The measured responsivity corresponds to a photoconductive gain (electrons flowing per incident photon) of 203. Another important parameter for UV photodetectors is response time. Figure 2c shows the time-resolved photocurrent of a ZnO nanoparticle film device in response to turn-on and turn-off of the UV illumination. The current of the device rises from 2.0 × 10^{-1} to 5.5 × 10^3 nA within 0.1 s, the time resolution of measurement, on illumination. The rapid photocurrent raise is followed by a slower component, in which the photocurrent increases by a further factor of 40 in about 25 s, before saturating. The photocurrent decay starts with a fast decay component during which the photocurrent drops by more than 3 orders of magnitude in the first 9−10 s after turning off the excitation. This fast

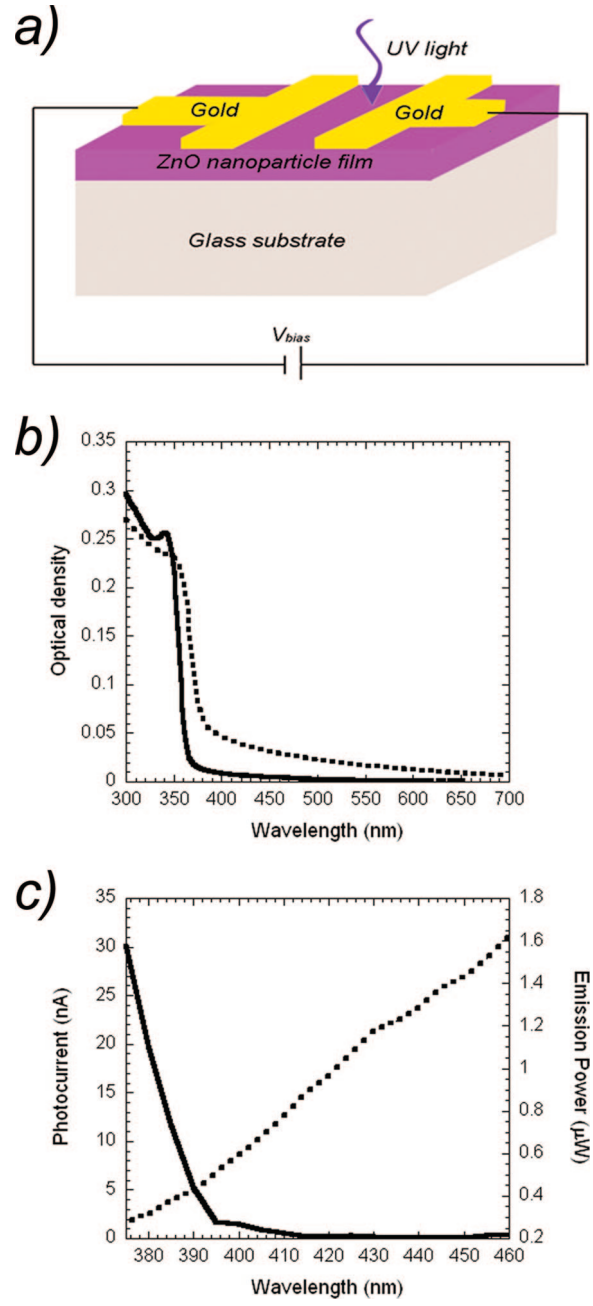

Figure 1. (a) Schematic of a ZnO nanoparticle film device structure (not to scale). (b) UV−vis absorption spectra of as-prepared ZnO nanoparticle solution (solid line) and a ZnO nanoparticle film after annealing (dashed line). (c) Photocurrent−excitation spectral response of a ZnO nanoparticle film device (solid line, left axis) and the corresponding emission spectrum from the tungsten lamp through a single-grating monochromator (dashed line, right axis). The photocurrents were calculated as $I_{illumination} - I_{dark}$, and both $I_{illumination}$ and I_{dark} were measured under 50 V bias.

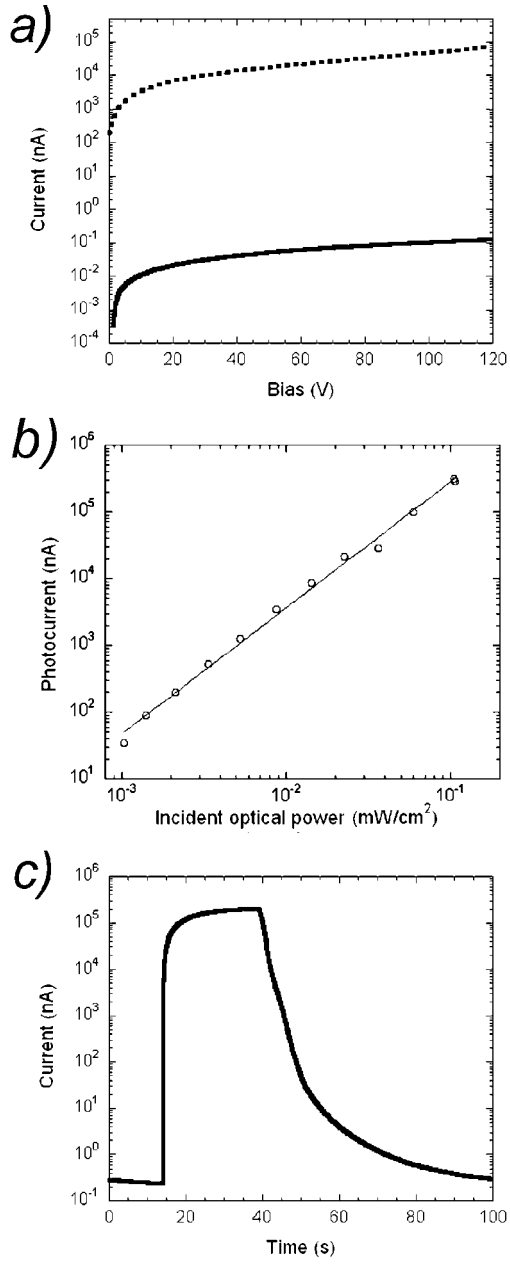

Figure 2. (a) Current versus voltage for a ZnO nanoparticle film device in the dark (solid line) and under 0.83 mW/cm^2 illumination at 370 nm (dashed line). (b) Photocurrent as a function of incident power at 370 nm at 120 V bias. Dark currents have been subtracted. For each power the current was allowed to stabilise for 2 min before measurement. (c) Time-resolved photocurrent at 120 V in response to a 25.5 s light pulse.

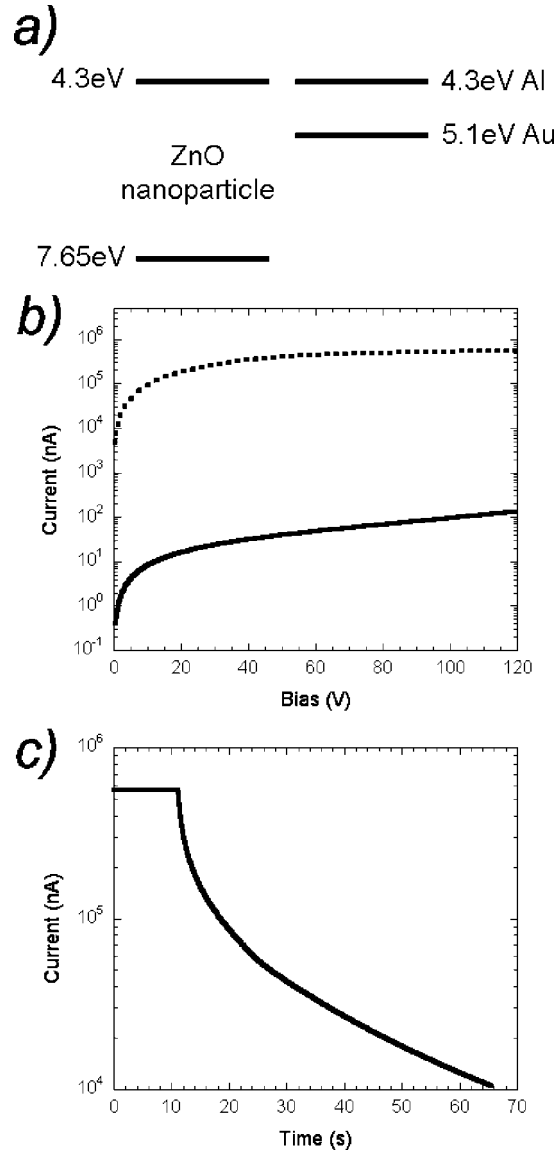

Figure 3. (a) Energy level diagram (relative to vacuum) for nanocrystalline ZnO relative to gold and aluminum work functions. (b) Current versus voltage for a ZnO nanoparticle film device with Al electrodes in the dark (solid line) and under 0.83 mW/cm^2 illumination at 370 nm (dashed line). (c) Photocurrent decay in a ZnO nanoparticle film device with Al electrodes at 120 V in response to turn-off of the UV illumination.

decay process follows a first order exponential relaxation function with an estimated time constant $\tau = 1.3$ s. A further slow photocurrent decay process lasts about 2 min during which the current decreases by another 2−3 orders of magnitude to reach its initial state.

Reproducibility of all results reported here was confirmed by fabricating three devices using nanoparticles from different synthesis batches. The ZnO devices were stable under ambient conditions since no degradation of device performance could be distinguished when the devices were stored in air for over 3 months.

The optical and electrical measurements provide insight into charge transport processes in ZnO nanoparticle film devices, including charge injection from metal contacts to ZnO nanoparticles and charge transport in the ZnO nanoparticle films. We note that the photoconductive gain in our devices is much larger than unity, so we require a mechanism where the photogenerated charges are not simply extracted from the device to produce the photocurrent, but instead cause some long-lived change in the device which causes further carriers to be injected and transported through the device.

It is generally accepted that oxygen molecules are adsorbed onto ZnO surfaces by capturing free electrons from the n-type ZnO [$O_2(g) + e^- \rightarrow O_2^-(ad)$] (Figure 4c), which creates a low-conductivity depletion layer near the surface.[7–18,29] These

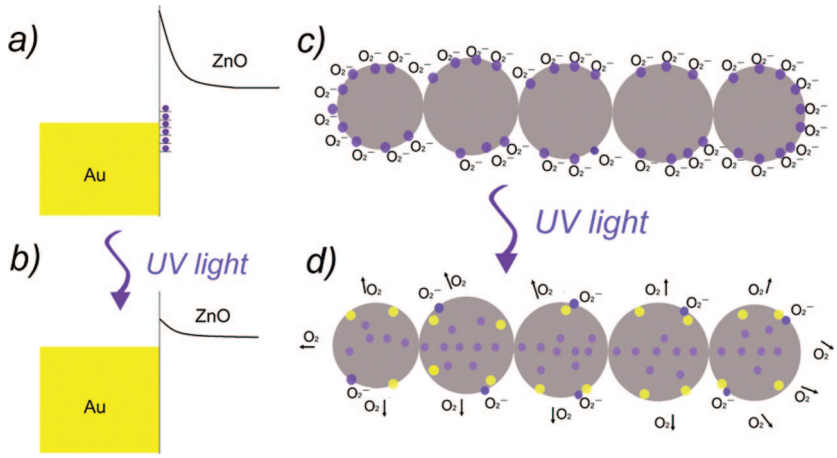

Figure 4. Carrier transport processes in the ZnO nanoparticle film devices. (a,b) Schottky barriers formed at the gold/ZnO nanoparticle interfaces in the dark and under UV illumination, respectively. (c,d) Charge carrier trapping and transport in the ZnO nanoparticle films in the dark and under UV illumination, respectively. Purple dots = electrons, and yellow dots = holes.

effects are particularly prominent in nanocrystalline films, where the surface area is large and the depletion regions may extend throughout the entire bulk of the film. These effects have also been observed in memory devices based on films of ZnO nanoparticles blended with polymer by Verbackel et al.,[30,31] who also observed enhanced conductivity on UV illumination. Upon illumination at photon energies above semiconductor bang gap (Figure 4d), electron−hole pairs are generated. The holes that migrate to the surface along the potential gradient produced by band-bending either discharge the negatively charged adsorbed oxygen ions [$h^+ + O_2^- \rightarrow O_2(g)$] to photodesorb oxygen from the surfaces or effectively get trapped at the ZnO nanoparticle surfaces, resulting in an increase in the free carrier concentration and a decrease in the width of the depletion layer. As we discuss in more detail below, this leads to an enhancement of carrier injection and transport, producing a persistent photocurrent. When the illumination is turned off, oxygen readsorbs on the nanocrystal surfaces, returning the device to its initial state. The very large surface to volume ratios of ZnO nanoparticle films which readily facilitate oxygen adsorption and desorption at the ZnO surfaces suggest that ZnO nanoparticles are superior candidates for UV detection based on a trapping mechanism related to gas adsorption and desorption. Measurements made in a nitrogen-filled glovebox show very long turn-off times of hundreds of seconds, consistent with the proposed oxygen readsorption mechanism.

It is important to distinguish between the effects of oxygen adsorption on carrier injection and those on carrier transport. In a device where the current is space-charge limited, it is easy to see that decreasing the trapping of free charges will lead to an increase in effective mobility and hence current. This effect is further enhanced in a disordered hopping system, where the mobility is strong dependent on free carrier density. While we believe that these "bulk" transport effects do play a role in our devices, experiments using different metal electrodes show that the photocurrent mechanism is in fact dominated by injection effects.

Figure 3a shows the approximate energy levels for ZnO nanoparticles relative to the workfunctions of gold and aluminum. For gold electrodes, which have been used in the experiments described above, it can be seen that there is a significant barrier to the injection of electrons into the ZnO. Formation of a Schottky contact is therefore expected. However, the existence of surface states at the ZnO/gold interface can significantly modify the injection barrier (Figure 4a). Because of the high density of trap states in our nanocrystalline films, classical methods to determine barrier heights[32] are difficult to apply. To demonstrate the influence of injection barriers on the current in devices using gold electrodes, we have therefore fabricated similar devices using a 70 nm thick aluminum layer as the electrodes instead of gold. Bulk Al/ZnO interfaces are found to be ohmic contacts because of the diffusion of aluminum into ZnO interface region during the thermal evaporation process.[6,33] It is expected that this diffusion process occurs more readily in our devices because of the large surface-to-volume ratio of ZnO nanoparticles, again forming ohmic contacts. Differences in device performance between devices with gold and those with aluminum contacts can therefore be attributed to the effect of an injection barrier at the gold/ZnO interface that limits the charge injection. Figure 3b shows the dark current and photocurrent of a device with aluminum electrodes under the same conditions as the device with gold electrodes shown in Figure 2a. The dark current with aluminum electrodes is 3 orders of magnitude larger than that with gold electrodes. The photocurrent is also increased, by about 1 order of magnitude. This shows that an injection barrier at the ZnO/Au interface controls the current, both in the dark and under illumination. The photocurrent must therefore arise primarily from changes in the injection process. A likely mechanism for this is that the presence or absence of adsorbed oxygen at the ZnO interface modifies the density of defect states and, hence, alters the injection barrier (Figure 4b). It is also possible that the high free charge densities present during illumination significantly reduce the width of the depletion layer. This mechanism is consistent

with the observed superlinear intensity dependence of the photocurrent, since the current is expected to respond superlinearly to changes in effective barrier height. Figure 3c shows the photocurrent decay in the device with aluminum electrodes, which drops by less than 2 orders of magnitude in 1 min. The more rapid photocurrent decay in the device with gold electrodes (Figure 2c) is consistent with the current being dominated by interfacial injection, where oxygen is only required to be readsorbed close to the interface to reduce the current.

In summary, we have demonstrated that solution-processed UV photodetectors can be conveniently fabricated using films of ZnO nanoparticles. The devices show low dark currents with a resistance >1 TΩ at room temperature as a consequence of the low free carrier density in the films in the absence of illumination. At wavelengths below 400 nm, a strong photocurrent is seen, with a responsivity of 61 A/W at an average intensity of 1.06 mW/cm^2 illumination at 370 nm. The characteristic times for rise and fall of the photocurrent are <0.1 s and about 1 s respectively, which may be adequate for applications that do not require particularly high speeds. The devices work reproducibly in air; indeed the adsorption and desorption of oxygen from the nanoparticle surfaces is essential to their operation. We have shown that the photocurrent is associated with a light-induced desorption of oxygen from the nanoparticle surfaces, thus removing electron traps and increasing the free carrier density. This reduces the Schottky barrier formed between the ZnO nanoparticle films and the gold contacts for electron injection, producing a persistent photocurrent. We suggest that, because of the very large surface-to-volume ratio, ZnO nanoparticle films are ideal materials for use in UV photodetectors that rely on a mechanism related to gas adsorption and desorption. Considering the advantages of solution-processable fabrication, the devices have potential for use in large-area UV photodetector applications.

Acknowledgment. This work was supported by the Engineering and Physical Sciences research Council, United Kingdom. J.W. is grateful to Cambridge Display Technology Ltd. for a studentship.

Supporting Information Available: Experimental details of the fabrication of "metal−semiconductor−metal" UV photodetectors. This material is available free of charge via the Internet at http://pubs.acs.org.

References

(1) Monroy, E.; Omnes, F.; Calle, F. *Semicond. Sci. Technol.* **2003**, *18*, 33–51.
(2) Goldberg, Y. A. *Semicond. Sci. Technol.* **1999**, *14*, R41−R60.
(3) Morkoc, H.; Strite, S.; Gao, G. B.; Lin, M. E.; Sverdlov, B.; Burns, M. *J. Appl. Phys.* **1994**, *76*, 1363–1398.
(4) Khan, M. A.; Shatalov, M.; Maruska, H. P.; Wang, H. M.; Kuokstis, E. *Jpn. J. Appl. Phys. Part 1-Regular Papers Brief Communications & Review Papers* **2005**, *44*, 7191–7206.
(5) Chen, C. H.; Chang, S. J.; Su, Y. K.; Chi, G. C.; Chi, J. Y.; Chang, C. A.; Sheu, J. K.; Chen, J. F. *IEEE Photonics Technology Letters* **2001**, *13*, 848–850.
(6) Liang, S.; Sheng, H.; Liu, Y.; Huo, Z.; Lu, Y.; Shen, H. *J. Cryst. Growth* **2001**, *225*, 110–113.
(7) Sharma, P.; Sreenivas, K.; Rao, K. V. *J. Appl. Phys.* **2003**, *93*, 3963–3970.
(8) Basak, D.; Amin, G.; Mallik, B.; Paul, G. K.; Sen, S. K. *J. Cryst. Growth* **2003**, *256*, 73–77.
(9) Takahashi, Y.; Kanamori, M.; Kondoh, A.; Minoura, H.; Ohya, Y. *Jpn. J. Appl. Phys. Part 1-Regular Papers Brief Communications & Review Papers* **1994**, *33*, 6611–6615.
(10) Murphy, T. E.; Moazzami, K.; Phillips, J. D. *J. Electron. Mater.* **2006**, *35*, 543–549.
(11) Zhang, D. H.; Brodie, D. E. *Thin Solid Films* **1995**, *261*, 334–339.
(12) Li, Q. H.; Gao, T.; Wang, Y. G.; Wang, T. H. *Appl. Phys. Lett.* **2005**, *86*, 123117–123119.
(13) Ghosh, R.; Mallik, B.; Basak, D. *Appl. Phys. A-Materials Science & Processing* **2005**, *81*, 1281–1284.
(14) Soci, C.; Zhang, A.; Xiang, B.; Dayeh, S. A.; Aplin, D. P. R.; Park, J.; Bao, X. Y.; Lo, Y. H.; Wang, D. *Nano Letters* **2007**, *7*, 1003–1009.
(15) Luo, L.; Zhang, Y. F.; Mao, S. S.; Lin, L. W. *Sensors Actuators A-Physical* **2006**, *127*, 201–206.
(16) Law, J. B. K.; Thong, J. T. L. *Appl. Phys. Lett.* **2006**, *88*, 113114–113116.
(17) Kind, H.; Yan, H. Q.; Messer, B.; Law, M.; Yang, P. D. *Adv. Mater.* **2002**, *14*, 158–160.
(18) Heo, Y. W.; Kang, B. S.; Tien, L. C.; Norton, D. P.; Ren, F.; La Roche, J. R.; Pearton, S. J. *Appl. Phys. A-Materials Science & Processing* **2005**, *80*, 497–499.
(19) Lao, C. S.; Park, M. C.; Kuang, Q.; Deng, Y. L.; Sood, A. K.; Polla, D. L.; Wang, Z. L. *J. Am. Chem. Soc.* **2007**, *129*, 12096–12097.
(20) Huynh, W. U.; Dittmer, J. J.; Alivisatos, A. P. *Science* **2002**, *295*, 2425–2427.
(21) Sirringhaus, H. *Adv. Mater.* **2005**, *17*, 2411–2425.
(22) Friend, R. H.; Gymer, R. W.; Holmes, A. B.; Burroughes, J. H.; Marks, R. N.; Taliani, C.; Bradley, D. D. C.; Dos Santos, D. A.; Bredas, J. L.; Logdlund, M.; Salaneck, W. R. *Nature* **1999**, *397*, 121–128.
(23) Konstantatos, G.; Howard, I.; Fischer, A.; Hoogland, S.; Clifford, J.; Klem, E.; Levina, L.; Sargent, E. H. *Nature* **2006**, *442*, 180–183.
(24) Pacholski, C.; Kornowski, A.; Weller, H. *Angewandte Chemie International Edition* **2002**, *41*, 1188–1191.
(25) Beek, W. J. E.; Wienk, M. M.; Janssen, R. A. J. *Adv. Mater.* **2004**, *16*, 1009–1013.
(26) Wong, H. M. P.; Wang, P.; Abrusci, A.; Svensson, M.; Andersson, M. R.; Greenham, N. C. *J. Phys. Chem. C* **2007**, *111*, 5244–5249.
(27) Sun, B.; Sirringhaus, H. *Nano Lett.* **2005**, *5*, 2408–2413.
(28) Sun, B. Q.; Sirringhaus, H. *J. Am. Chem. Soc.* **2006**, *128*, 16231–16237.
(29) Liao, Z. M.; Liu, K. J.; Zhang, J. M.; Xu, J.; Yu, D. P. *Phys. Lett. A* **2007**, *367*, 207–210.
(30) Verbakel, F.; Meskers, S. C. J.; Janssen, R. A. J. *Appl. Phys. Lett.* **2006**, *89*, 102103–102105.
(31) Verbakel, F.; Meskers, S. C. J.; Janssen, R. A. J. *J. Phys. Chem. C* **2007**, *111*, 10150–10153.
(32) Clifford, J. P.; Johnston, K. W.; Levina, L.; Sargent, E. H. *Appl. Phys. Lett.* **2007**, *91*, 253117.
(33) Kim, H. K.; Kim, K. K.; Park, S. J.; Seong, T. Y.; Adesida, I. *J. Appl. Phys.* **2003**, *94*, 4225–4227.

NL0803702